Int. J. Multiphase Flow Vol. 8, No. 5, pp. 459–473, 1982
Printed in Great Britain.

0301-9322/82/050459-15$03.00/0
Pergamon/Elsevier

# TWO-PHASE MEASUREMENTS OF SALTATING TURBULENT BOUNDARY LAYER FLOW

B. R. WHITE
Department of Mechanical Engineering, University of California, Davis, CA 95616, U.S.A.

(*Received* 15 *September* 1981; *in revised form* 8 *January* 1982)

**Abstract**—Mean wind and particle speed measurements as functions of height were made for a saltating turbulent boundary layer flow. An exponential dependence of particle flux with height above the surface was found independent of windspeed and particle size. Particle-speed distributions as functions of height above the surface were measured for experiments conducted at two ambient pressures: atmospheric pressure and approximately 1% atmospheric pressure. The wind was shown to be a more efficient mover of particles at atmospheric pressure.

High-speed motion pictures of saltating ground walnut shells (of diameter 500–1500 $\mu$m and density 1.1 g/cm$^3$) were taken in an environmental wind tunnel to simulate the planetary boundary layer. These experiments verify the existence and magnitude of particle spin rates proposed by White & Schulz (1977). There was remarkable agreement between numerical trajectory solutions, including the spin effect, and the filmed trajectories. An observation was made that not all particles spin exclusively in the vertical longitudinal plane (in the direction of flow). At low pressures (0.6 kPa) the effect of spin forces on the particle's trajectory was shown to have little influence and was verified by a theoretical force ratio balance of spin to drag force.

## 1. INTRODUCTION

The transport of an unsuspended solid over a gravity bed by wind action is known as saltation. The wind causes individual particles to move in a series of short ballistic-type trajectories, basically uninfluenced by the wind's turbulence. Gilbert (1914) first used the term saltation, derived from the Latin verb *saltare* meaning "to leap or dance," as a description of the motion of sand particles under water.

Relatively few experiments have been reported that investigate the motion of individual saltating particles (e.g. trace out their trajectories) and none that presented particle velocity distributions as functions of height above the gravity bed. The lack of this experimental data has been, apparently, due to the lack of appropriate means to acquire useful data. However, the overall characteristics of saltation have been determined by experiments and described by several workers (Free 1911; Bagnold 1941, 1956; Chepil 1945, 1958; Kawamura 1951; Zingg 1953; Williams 1964). Some aspects of particles' trajectories have been investigated by Bagnold (1973, 1974), Francis (1973), and Abbott & Francis (1977). Abbott & Francis presented particle trajectories occurring in water. Further, White & Schulz (1977) presented saltation trajectories in air and estimated particle spin rates from 115 to 500 rev/s.

Analytical studies of saltation also have been scarce. Kawamura (1951) presented an analytical theory for predicting material flux rates. An analytical solution for saltation was developed by Owen (1964), and the solution was applied to drifting snow by Radok (1968). Tsuchiya (1969) developed a theoretical analysis on the successive saltating leaps of particles. Bagnold (1973) and Sagan & Bagnold (1975) presented approximate analysis of saltation that unified results of water and air saltation. Andres (1970), Maegley (1976), Iversen *et al.* (1973, 1975, 1976), White *et al.* (1976), and White (1979a, 1981) reported numerical solutions and predictions about saltation as applied to the planets Mars and Venus.

None of the experimental work given above, or any other literature known to the author, presented particle-speed distributions occurring in saltation, which is the purpose of the present investigation. Another purpose of the present work is to verify the assumed spinning rates used by White & Schulz (1977), through the study and evaluation of high-speed motion-picture films.

## 2. WIND-TUNNEL FACILITY AND INSTRUMENTATION

The test facility is a low-pressure chamber located at NASA Ames Research Center, Moffett Field, California. The chamber houses an atmospheric wind tunnel. The tunnel occupies the center floor area of the chamber. The present test section provides a zero-pressure-gradient test facility. The pressure chamber allows variation in the ambient pressure from atmospheric pressure to approximately 1% atmospheric pressure. During any experiment the ambient pressure is held constant. Vacuum to the low-pressure chamber is supplied from a five-stage stream ejector plant.

The wind tunnel is a $1.2 \times 0.9$ m open-circuit type with a total length of about 13 m. It consists of five sections, each 2.4 m long, plus a 1 m entrance, see figure 1. The first section is wood enclosed and contains the entry section and flow straighteners. The following two sections are constructed of 2.4 cm-thick Plexiglas on all sides. All measurements are taken in the third section at a distance of 6.36 m from the entrance. The fourth and fifth sections are diffusers.

A boundary layer trip of 1 cm diameter pebbles is randomly placed over the first meter of the tunnel's floor adjacent to the entrance section. The remaining portion of the tunnel's floor is covered with rigidly attached 500 $\mu$m mean diameter sand particles. The test section is more than 25 boundary layer lengths from the pebble trip. A fairing of concave molding is installed in the four corners of the tunnel to reduce secondary flows. A flow straightener (section A–A of figure 1) is used in the tunnel entry. It is constructed 25 cm wide by 0.1 cm thick with $10\,\text{cm} \times 10\,\text{cm}$ openings. This results in a free-stream turbulence level of 2%. A complete description of the test facility is given in by White (1979b).

The tunnel is drive by high-pressure air ejected through a network of small orifice nozzles located at the end of tunnel section 4. There are thirteen pipes, each with 5 or 6 orifices yielding a total of 72 equally spaced orifices (section C–C of figure 1). The maximum freestream wind speed through the tunnel is 15 m/s at atmospheric pressure and 170 m/s at 0.5 kPa pressure, where freestream speed is the wind speed measured at the mid-height in the wind tunnel.

Mean velocity profiles are measured by means of a flattened-tip Pitot tube designed by United Sensor. A 3.2 mm diameter static pressure probe is mounted near the Pitot tube in the same downstream plane. The Pitot tube is mounted on a rack and pinion vertical transversing device (section B–B of figure 1). The pressure differential is measured by a Datametrics

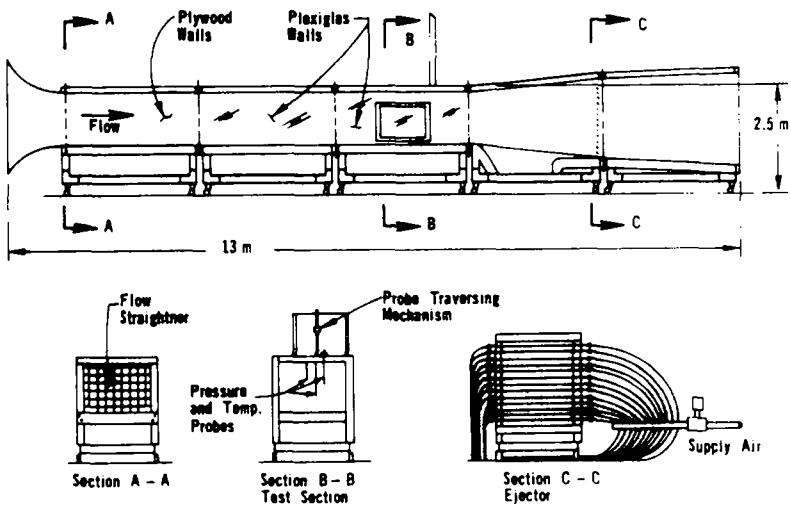


Test Section Area = 1.1 $m^2$

Figure 1. Schematic diagram of the open-circuit wind tunnel showing entrance section and flow straighteners (section A-A), test section with various probes (section B-B), and diffuser drive system (section C-C).

Barocel. For increased accuracy in determining the mean-velocity profiles, MacMillan's (1954, 1956) low-Reynolds-number and shear displacement corrections are applied to the Pitot-tube measurements. The maximum corrections applied to the Pitot-tube measurements are always less than 5% of the resultant velocity. Further, it is assumed that the Pitot tube responds only to the longitudinal component of turbulence.

Particle speed is determined with a velocimeter based on a design developed by the U.S. Rocky Mountain Forest Service (Schmidt 1977). It produces a light beam exposed perpendicular to the wind stream and two light-sensitive semiconductors that detect the shadow of any intersecting particle as it crosses two separate portions of this light beam (figure 2). Parallel windows limit the view of the light receivers; an amplifier connects the two phototransistors such that a particle passing through the light beam produces a positive voltage pulse as it shadows the first window, and a negative pulse at the second window. To determine particle speed, the time interval between positive and negative pulses is tape recorded (Hewitt–Packard Model No. 3950) and replayed through a Honeywell filter optics-cathode ray tube visicorder (Model No. 1856A). This procedure produces very accurate ($\pm 2\%$) estimates of time intervals. The time interval, in conjunction with the known separation distance of the sensor windows, enables the particle velocity to be determined. An average of 500 consecutive particles passing through the windows are reduced for each height to form the particle speed distributions.

## 3. MATERIAL FLUX AND PARTICLE SPEED DISTRIBUTIONS

Wind-tunnel experiments are performed using particle collectors to determine the material flux as a function of height $y$ above the surface. The flux measurements are made in conjunction with particle velocity measurements which then determine particle speed distributions and relative particle flux concentrations as functions of height. The experiments are performed at two ambient chamber pressures, one at 0.66% atmospheric pressure and the other at atmospheric pressure. Two particle sizes are tested. One is common quartz "sand", mean diameter of 715 $\mu$m, which has a particle-size distribution from 500 to 1000 $\mu$m, and the other sieved quartz "sand", mean diameter of 92 $\mu$m, which has a narrow particle-size distribution (from 80 to 120 $\mu$m diameter particles). The 92 $\mu$m sized particles are known to be the most easily moved by the lowest strength wind (Bagnold 1941). For both sized particle distributions, experiments are performed at two speeds, one just above saltation threshold speed, and the other substantially above threshold speed. Particle velocity distributions are measured at approximate heights of 30, 70, 160, 240, and 500 mm. The boundary layer is approximately 200 mm thick at the test section.

No particle collector is 100% efficient for collection of saltating particles. Thus, the particle collector used in the present experiment is designed to minimize wind flow interference and to maximize particle collection. The optiminization of geometry of particle collectors is ac-

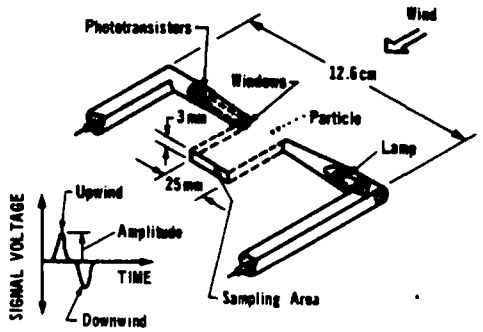


Figure 2. Schematic diagram of particle velocimeter. Device consists of a light source and two microphototransistors. As a particle passes through the beam, the upwind phototransistor registers a positive voltage, then the second (downwind) phototransistor registers a negative voltage; the difference between the two signals yields time (hence, velocity). This device is based on a design modified from Schmidt (1977).

complished by flow visualization tests in a smoke tunnel. The present design provides minimum flow disturbance while collecting the majority of the saltating particles, i.e. all particles above 40 $\mu$m diameter. As shown in figure 3, the particle collection system consists of 100 individual 1 cm-high stackable Plexiglas collectors. Each collector has approximately a 1 cm$^2$ frontal cross section area which expands five fold on the downstream side of the collector and has a wire mesh for the back wall. The back wall mesh spacing allows wind and mean sized particles of 40 $\mu$m diameter or less to pass through it. The air flow through the rear wall area of the collectors prevents separation from occurring off the sharp-edged intersection of the side wall with rear wall. High-speed movies show particles to be efficiently trapped with only a few particles greater than 40 $\mu$m rebounding out of the collector.

Once the particles are caught in the individual traps, the material of each trap is separately weighed yielding the flux as a function of height. Great care is taken to accurately measure the length of the saltation time to which each collector is exposed for calculation of the flux rates.

Figure 4 displays the particle flux, $\hat{q}$, grams of material passing through a vertical area per unit time in units of g/(cm$^2$-s) as a function of height $y$ above the surface. The hollow symbols are the atmospheric pressure cases; the solid symbols are the low pressure cases. It is interesting to note that logarithm of $\hat{q}$ is proportional to the height regardless, apparently, of the windspeed, particle size, and ambient pressure (except near the surface $y < 5$ cm). The approximate linearity of the curves displayed in the figure imply an exponential dependence of $\hat{q}$ upon height. Near the surface the particle motion is primarily due to surface traction.

It was feared that the saltating particles may have been rebounding off the wind tunnel ceiling. In order to assess the ceiling effect on the collectors, particles were collected in 2 cm intervals from the floor to the ceiling. A typical result is shown in figure 5 where above 65 cm

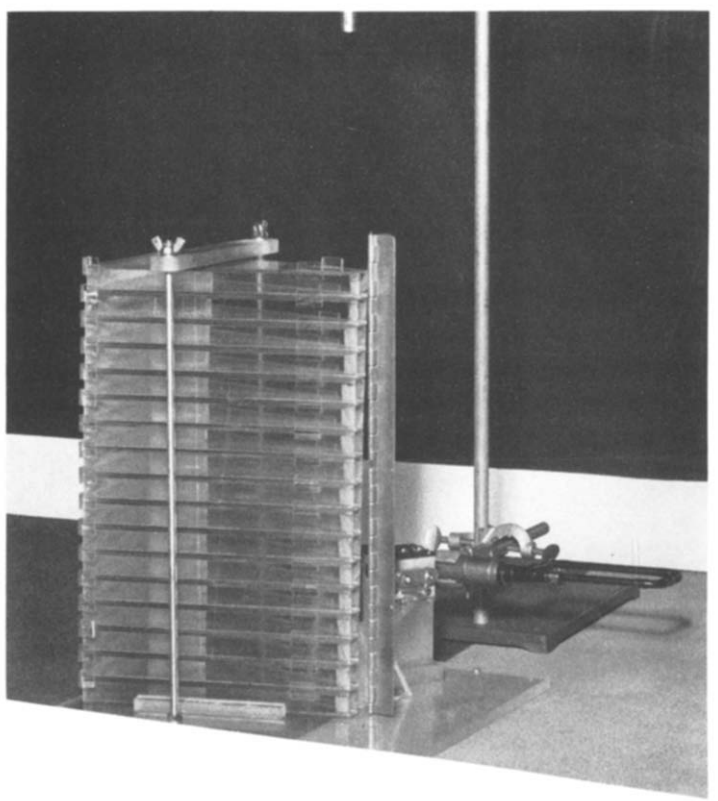

Figure 3. View of particle collectors used to determine flux of saltating grains. Samples are taken for approximately 1 cm$^2$ cross section area, at intervals of 1 cm above the floor. Collector was designed for maximum efficiency of particle collection for grains 40 $\mu$m and larger, with minimum interference of flow. Also shown is particle velocimeter.

there are erratic values of $\hat{q}$, evidently as a result of particles bouncing off the ceiling. As a result of this behavior, and the fact that very few particles are caught above 65 cm by the collectors, only data up to a height of 65 cm are shown.

The particle speed distributions are determined at constant height locations by means of the velocimeter described earlier (Schmidt 1977). A typical low pressure result for the 92 $\mu$m size particles is shown in figure 6. In general, there is an increase in mean particle velocity with increasing height above the surface reflecting the increasing windspeed through the boundary layer. The particle speed distributions measured at a particular height arise because the

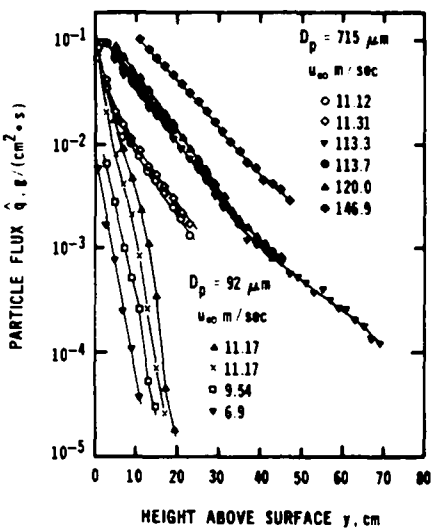


Figure 4. Particle flux as a function of height above the surface for two average grain sizes for a range of freestream velocities ($u_\infty$). Open symbols are one atmosphere runs; dark symbols are low pressure runs (0.65% atmospheric pressure).

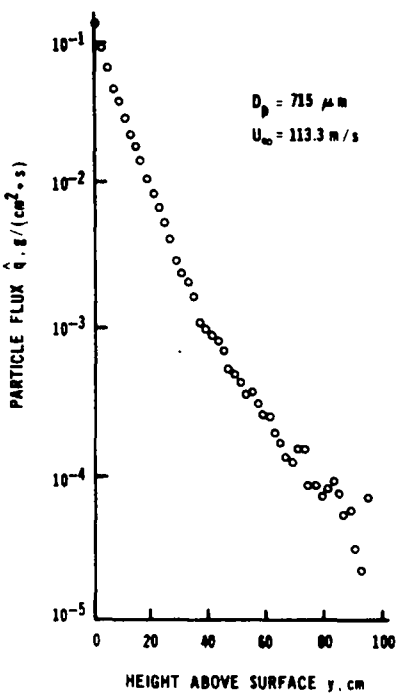


Figure 5. Typical data set of particle flux as function of height above surface, from which figure 4 was derived, showing the possible effect of the wind tunnel ceiling. Wind tunnel is about 0.9 m high. Scatter in data about 65 cm is probably due to saltating grains bouncing from the ceiling.

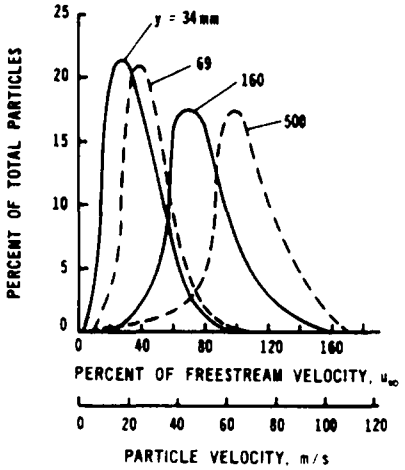


Figure 6. Distribution of velocities of particles 92 $\mu$m in diameter for four heights at a freestream speed, $u_\infty$ of 63.9 m s$^{-1}$, at 0.60% atmospheric pressure.

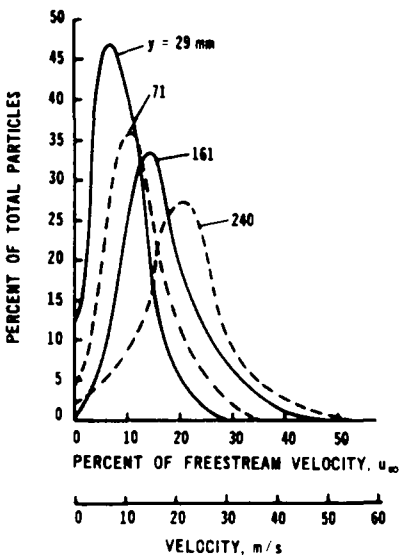


Figure 7. Distribution of velocities of particles 715 $\mu$m in diameter at four heights at a freestream speed ($u_\infty$) of 115 m/sec, at 0.66% atmospheric pressure. Velocity is given both as *m/s* and as a percentage of freestream.

measured particles at this height can all be at different stages of their individual trajectories (could be rising or falling) as well as random differences due to the saltation process. Each curve shown on the figure is the statistically averaged analysis of a minimum of 500 consecutive particles passing through the velocimeter. An interesting result occurs at the 160 mm and 500 mm locations, where particle speeds are measured that exceed the freestream speed. This phenomenon is most likely due to favorable particle collision in mid-flight that catapults particles downstream at speeds greater than freestream velocity, $u_\infty$. This result does not seem spurious, as it is repeatedly observed.

Figure 7 displays the low pressure particle speed distributions for the 715 $\mu$m size particles. The mean particle speed increases with increasing height; however, expressed as a percentage of the freestream velocity it is substantially greater than that observed with the 92 $\mu$m size distribution particle for the same heights. Although for both tests at low pressures there are more particles near the mean speeds at heights of 29 and 71 mm for 715 $\mu$m size particles, they are not as efficiently accelerated by wind action as 92 $\mu$m size particles.

Figure 8 displays the mean particle speed results extracted from figure 7 as well as the similar results of the atmospheric pressure case (particle speed distributions not shown). The atmospheric pressure experiment uses the same 715 $\mu$m size material and it is performed under dynamically similar conditions, i.e. both low and high pressure experiments have the same ratio of freestream speed to particle threshold freestream speed (White 1979a). The lack of coupling with the wind at low pressure is observed when compared to the more efficient acceleration of particles at atmospheric pressure. Winds at higher ambient pressures are more efficient transporters of material in saltation than at lower ambient pressures, both under equal dynamic conditions.

Mean wind velocity profiles were obtained with and without saltation. Figure 9 shows the typical mean velocity profile as a function of height without saltation. The freestream speed is 82.6 m/s. The mean velocity profile is well governed by the equation (shown as the straight line on the figure)

$$\frac{u}{u_*} = \frac{1}{K} \log (y/y_0)$$

which yields a value of $y_0 = 0.180$ mm and friction speed of $u_* = 5.12$ m/s. Figure 10 shows approximately the same freestream speed with saltation of the 92 $\mu$m diameter quartz particles. Two straight solid lines are drawn through the data according to the method described by Bagnold (1941) to determine the equivalent roughness height in saltation $y_0'$ which is 54 mm. However, the $u_*'$, equal to 11.4 m/s, is more than twice as great as figure 9. Also shown on the figure is the mean velocity profile without saltation (dashed line). According to Bagnold (1941), the upper solid line should be parallel to the dashed line which was found to be approximately true at atmospheric pressure. This situation is not found to exist in the low pressure data, and the data displayed in figures 9 and 10 are typical of all low pressure profiles taken with and without saltation present. This fact suggests that the difference between the present low pressure measurements and those of Bagnold lies only in the change of ambient pressure.

## 4. EFFECT OF PARTICLE SPIN

The spinning of particles in saltation at atmospheric pressure are shown to have a profound influence on the resulting trajectories (White & Schulz 1977). The purpose of this section's experiments are to verify the high spin rates of saltating particles. The pressures at which the experiments are performed are approximately 0.68% atmospheric pressure, one-half atmos-

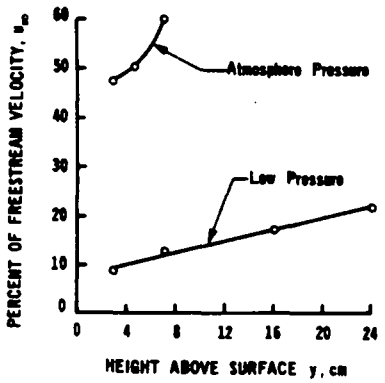


Figure 8. Average velocity of particles 715 $\mu$m in diameter as a function of height above surface at atmospheric pressure and at 0.65% atmospheric pressure. Both cases are run at freestream speeds just above saltation threshold (11.1 m/s and 112.5 m/s). Note that at atmospheric pressure particles achieve about half the velocity of freestream, whereas at low pressure the grains achieved only about 1/5 freestream speed.

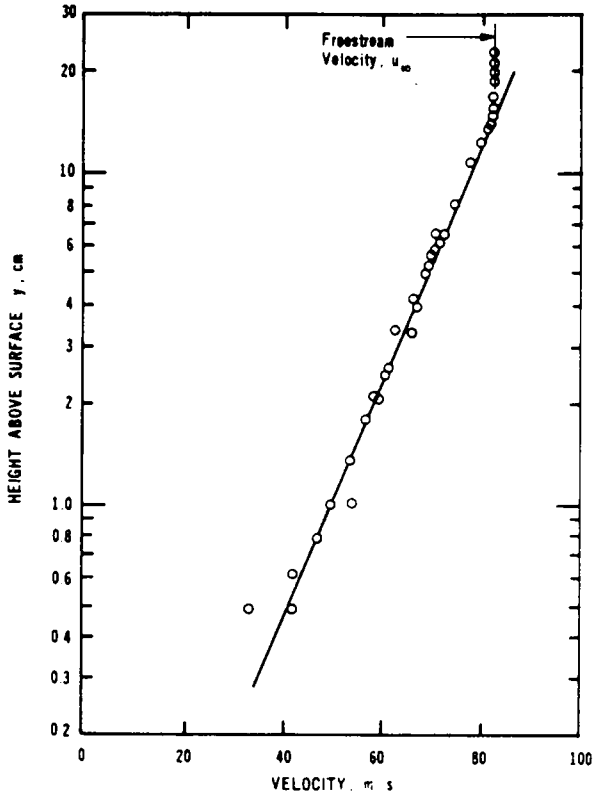


Figure 9. Mean velocity profile as a function of height above the surface for a freestream velocity of 82.6 m/s at 0.6% atmospheric pressure. $u_* = 5.12$ m/s.

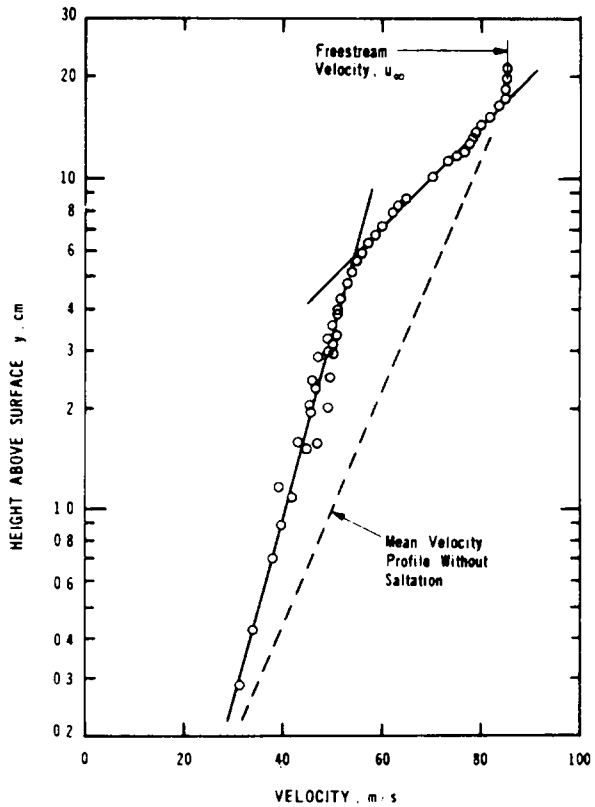


Figure 10. Mean velocity profile as a function of height above the surface with saltation of 92 $\mu$m size particle present at 84 m/s at 0.6% atmospheric pressure. Also shown (dashed line) is the mean profile without saltation from figure 9.

pheric pressure, and atmospheric pressure. The investigation of the particle motion is accomplished through the study and evaluation of high-speed motion pictures taken in the wind tunnel. The filmed trajectories are then compared with trajectories obtained by numerical integration of the equations of motion including the spin effect.

*Wind-tunnel experiment*

The saltating material is ground walnut shell with a density 1.1 g/cm$^3$. The selection of ground walnut shell is made to serve two purposes. The shape of ground walnut shell is similar to that of natural windblown materials (Greeley *et al.* 1977). Secondly, the non-circular geometry of individual particles make measurements of rotation rates possible.

The high-speed motion pictures are taken with a Nova camera at 2,000–10,000 frames/s in the downstream section of the tunnel. The camera is pointed horizontally and perpendicular to the direction of flow such that the flow and the saltating particles travel from left to right across successive frames. The flow is lit by several high intensity mercury-arc lamps so that particles moving in a narrow (1–2 cm wide) vertical plane aligned with flow direction are illuminated and hence visible on the film. A centimeter grid on the far side of the flow provides a spatial reference frame which permits subsequent determination of the position of individual particles. In order to have accurate film resolution to be able to measure both the particle's position and spin simultaneously, a rather restrictive camera field of view had to be utilized, which was 6 cm high by 10 cm long. This field of view enables only the lifting-off particles to be filmed. The particles returning to the surface travel at greater speeds than those particles lifting off. Even at the maximum film rate of 10,000 frames/s it was not possible to accurately observe these particles. This limitation is an inherent problem in filming small particles in motion over relatively large distances.

Before each filmed experiment, a layer of ground walnut shell is spread on the wind-tunnel floor, carefully smoothed out, and leveled to a height of 1 cm. The floor area covered is approximately 10 cm by 200 cm, the longer dimension being in the direction of the flow.

Viewing of the film is on a Vanguard Motion Analyzer. The film could be run through this device forward or backward, either at a continuous variable speed, or frame by frame. A frame counter makes it possible to keep track of position within the section of film being viewed. The film is projected onto a flat frosted-glass surface. The particle's trajectory is easily traced out by manually advancing the film. A stroke light device leaves a light flash at 0.001-second intervals on the margin of the film which permits a precise determination of the film speed. Hence, along with tracing out a path of an individual particle, a simultaneous determination of the particle spin is made.

Of the 60 particle trajectories traced out, 24 are at atmospheric pressure, 7 are at approximately 50% atmospheric pressure, and 29 are at 0.68% atmospheric pressure.

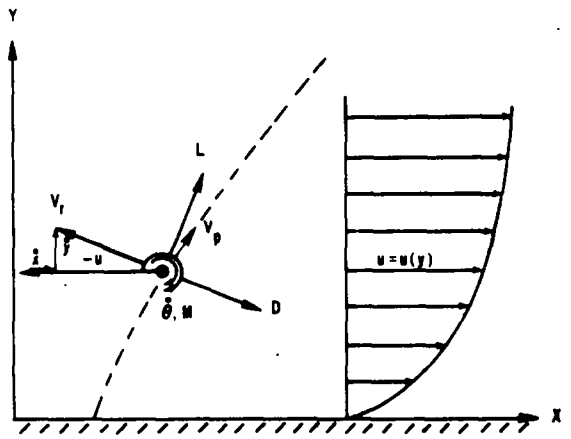


Figure 11. Forces and velocities associated with a saltating particle.

*Numerical solutions*

For the numerical solutions to the equations of motion, a one-dimensional flow situation is assumed in which the velocity in the vertical ($y$) direction is zero and the velocity $u$ in the flow ($x$) direction is the measured velocity profile as a function of height obtained from the saltation experiments. The typical saltating particle and flow geometry are shown in figure 11. The equations of translational and rotational motion of a particle are written as (White & Schulz 1977):

$$m_p\ddot{x} = L\dot{y}/V_r - D(\dot{x} - u)/V_r$$

$$m_p\ddot{y} = L(u - \dot{x})/V_r - D\dot{y}/V_r - m_p g$$

$$I_p\ddot{\theta} = M$$

where $m_p$ is the particle's mass, $I_p$ is the particle's moment of inertia, $\ddot{\theta}$ is the particle's angular acceleration, $D$ is the drag force, and $\dot{x}$, $\dot{y}$, $\ddot{x}$, and $\ddot{y}$ are the particle's velocity and acceleration. The relative velocity $\bar{V}_r$ is defined as $\bar{V}_{\text{particle}} - \bar{V}_{\text{air}}$ where $\bar{V}_{\text{particle}}$ is the vector velocity of the particle and $\bar{V}_{\text{air}}$ is the vector velocity of the air flow, and the drag force is in the direction opposite to the relative velocity vector. The magnitude of the relative velocity is expressed in terms of the particle and flow velocity components as

$$V_r = [(\dot{x} - u)^2 + \dot{y}^2]^{1/2}.$$

The work of Rubinow & Keller (1961) is used in estimating the particle moment and resultant lift force developed from the rotation of the particle. The lift and moment are

$$L = \pi/8 D_p^3 \rho V_r(\dot{\theta} - \tfrac{1}{2}\partial u/\partial y)$$

$$M = \pi\mu D_p^3(\tfrac{1}{2}\partial u/\partial y - \dot{\theta})$$

where $\dot{\theta}$ is the particle's angular velocity and $\mu$ is the absolute viscosity of the fluid. These equations are valid only for the case of vanishingly small Reynolds number. Their use in the present case is justified by the fact that it is desired primarily to find out whether the addition of terms accounting for particle spin will significantly improve the agreement between theory and experiment.

The equations of motion are solved numerically by a computer. The solving scheme is an initial-value ordinary-differential-equation solver using a predictor–corrector computation algorithm. The initial values (position, velocities, and spin rate) are obtained from experimental measurements taken in the wind tunnel at the beginning of each of the particles' trajectory. The empirical drag coefficients of Morsi & Alexander (1972) are used to calculate the drag coefficient needed in the numerical integration.

*Atmospheric pressure results*

Figure 12 displays a typical comparison between the filmed path traced out by a particle with two theoretical solutions. The first solution is with no spin, and the second solution is with the experimentally measured spin rate of 483 rev/s. The plane of spin appears to be entirely in the vertical longitudinal plane as is the particle motion. Good agreement is found between the filmed trajectory and the numerical solution with particle spin. The measured and calculated particle speeds along the trajectory were essentially the same for the solution with particle spin. The drag only comparison had poor agreement.

In many other trajectories, the particle spin is not entirely in the vertical longitudinal plane

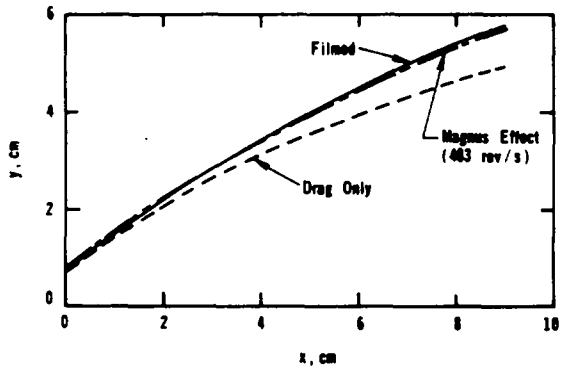


Figure 12. A comparison of a filmed (solid line) path traced out by a particle with theoretical calculations (dashed lines) from the equations of motion with and without measured particle spin of 483 rev/s. The particle was approximately 600 $\mu$m, and $u_* = 29.9$ cm/s at atmospheric pressure.

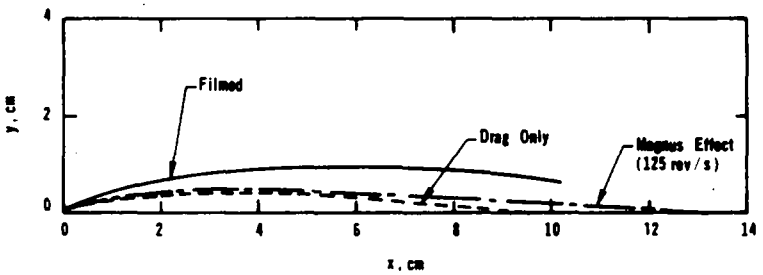


Figure 13. A comparison of a filmed (solid line) path traced out by a particle with theoretical calculations (dashed lines) from the equations of motion with and without particle spin rate of 125 rev/s measured in the vertical longitudinal plane (in the flow direction). Here the true spin plane was not the vertical longitudinal one, thus the measurement underestimates the true spin rate. The particle was approximately 600 $\mu$m, and $u_* = 29.9$ cm/s at atmospheric pressure.

as is the particle motion. Perhaps this effect is due to the particle colliding with surrounding particles on the surface as it lifts off or rebounds from the surface. Figure 13 displays a filmed trajectory where the spinning of the particle is known to be not entirely in the vertical longitudinal plane. It is impossible to precisely determine the exact plane of particle spin. In figure 13, the theoretical solution (with the experimentally measured spin rate of 125 rev/s) falls below the filmed particle path. The plausible explanation is that the experimentally measured spin rate is only that of the vertical longitudinal plane and is only a fraction of its true value. The same result was found by Abbott & Francis (1977) for particle motion in water. This phenomenon occurs in approximately 20% of all saltating particles observed.

*One-half atmospheric pressure results*

An analysis of the seven particle trajectories recorded at approximately one-half atmospheric pressure (49.3 kPa) exhibits similar correlation as those filmed at atmospheric pressure. The typical outcome of this is shown in figure 14. Here, the particle spin appears to be entirely in the vertical longitudinal plane, and it is measured at 400 rev/s. The numerical solutions with and without spin are presented. Again, good agreement is present between the theoretical solution with spin and the filmed trajectory including comparison between the measured and calculated particle speeds along the trajectory.

*Low-pressure results*

At an ambient chamber pressure of 0.68 kPa, 29 individual particle trajectories are traced from the films. The filmed trajectories are compared with the numerical solutions with and without particle spin rates. Typical sets of trajectories for the low-pressure experiment are

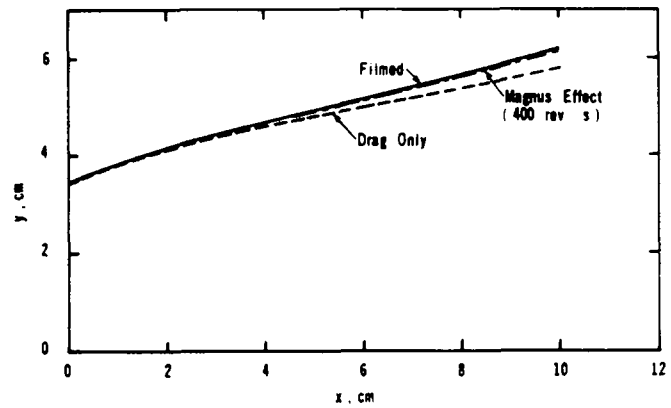


Figure 14. A comparison of a filmed (solid line) path traced out by a particle with theoretical calculations (dashed lines) from the equations of motion with and without measured particle spin rate of 400 rev/s in the vertical longitudinal plane. The particle was approximately 700 $\mu$m, and $u_* = 45.4$ cm/s at 49% atmospheric pressure.

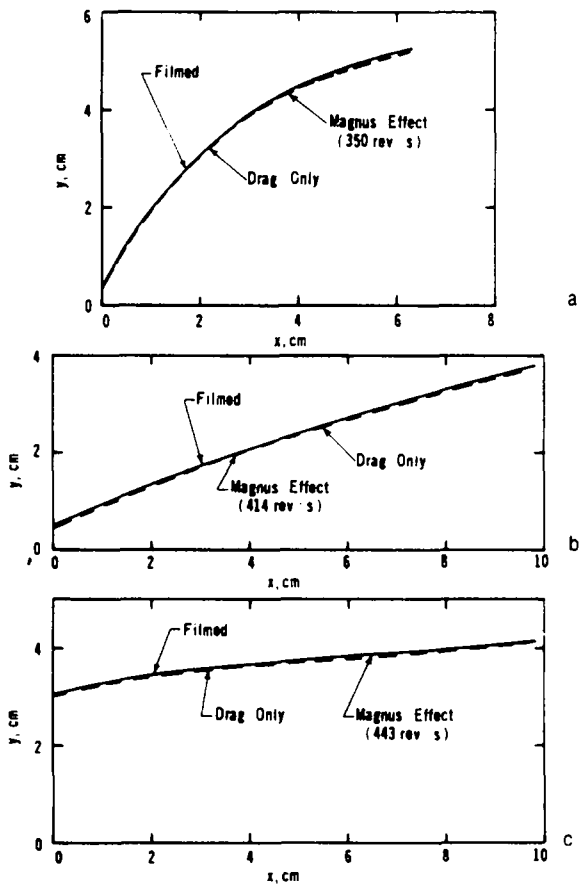


Figure 15. A comparison of filmed (solid line) path traced out by a particle with theoretical calculations (dashed lines) from equations of motion with and without a measured particle spin rate of (a) 350 rev/s, (b) 414 rev/s, and (c) 443 rev/s in the vertical longitudinal plane. The particles were all approximately 1200 $\mu$m, and $u_* = 436$ cm/s at 0.68% atmospheric pressure.

presented in figures 15(a)–(c). The agreement between theory and experiment is essentially independent of the spin rate. There is only a 1–3% difference between the numerical and filmed trajectories. This phenomenon is present in all 29 trajectories reduced. The measured and calculated particle speeds along the trajectories were essentially all the same regardless of particle spin rate.

This result is explained by an examination of the spin lifting force $L_S$ and drag $D$ at low pressure which are,

$$L_S = \frac{\pi}{8} D_p^3 \rho V_r \left(\dot{\theta} - \frac{1}{2}\frac{\partial U}{\partial y}\right)$$

$$D = \frac{\pi}{8} D_p^2 \rho V_r^2 C_D.$$

Experimentally, for both high and low pressure at particle lift-off, near but not on the surface, the particle spin rate is much greater than the shear rate of the flow ($\dot{\theta} \gg \partial U/\partial y$). Thus, the spin lift to drag ratio is equal to

$$\frac{L_S}{D} = \frac{D_p \dot{\theta}}{V_r C_D}$$

A sensible result of the experimental data shows the average initial spin rates of both low pressure and atmospheric pressure tests to be approximately equal; 387 rev/s with a standard deviation of 138 rev/s (24 particles) for low pressure, compared to 346 rev/s with a standard deviation of 123 rev/s (29 particles) for atmospheric pressure. Note the spin moment depends only on absolute viscosity and not fluid density, as does the spin lift.

The importance of the spin force is found by examining its magnitude compared to the magnitude of the drag force at low pressure, $(L_S/D)_{low}$ and comparing the ratio to the same ratio at atmospheric pressure $(L_S/D)_{atm}$. The ratio of $(L_S/D)_{low}$ at low pressure to ratio of $(L_S/D)_{atm}$ at atmospheric pressure is expressed as

$$\frac{\left[\frac{L_S}{D}\right]_{low}}{\left[\frac{L_S}{D}\right]_{atm}} = \left[\frac{V_{r_{atm}}}{V_{r_{low}}}\right]\left[\frac{C_{D_{atm}}}{C_{D_{low}}}\right].$$

For dynamical similarity conditions, $V_r^2 \sim \rho$, (White 1979a) this equation becomes

$$\frac{\left[\frac{L_S}{D}\right]_{low}}{\left[\frac{L_S}{D}\right]_{atm}} = \left[\frac{\rho_{low}}{\rho_{atm}}\right]^{1/2}\left[\frac{C_{D_{atm}}}{C_{D_{low}}}\right].$$

If the spin forces are of equal importance in determination of the particles' trajectory at low pressure, then the ratio in the above equation would have to be unity. This ratio shows that the spin effect on trajectories at low pressure is negligible, since the ratio is very small compared to unity. The density ratio $\rho_{low}/\rho_{atm}$ is approximately 1/200. The $C_D$ ratio is less than unity, $C_{D_{atm}} < C_{D_{low}}$, since the $C_D$ is only a function of Reynolds number. Hence, spin effects are shown to be unimportant at low pressure.

## CONCLUSIONS

The logarithm of particle flux $\hat{q}$ as a function of height were found to be linearly related to the height regardless, evidently, of the wind speed, particle size, and ambient pressure, thus implying an exponential dependence of $\hat{q}$ with height. Particle-speed distributions as a function of height demonstrated a better coupling of particle speed to the wind speed at atmospheric pressure than at low pressure. Further, some particles at heights at the edge and outside the

boundary layer were found to have speeds greater than freestream speed at low pressure, evidently as a result of a favorable collision that propelled them in a downstream direction.

High-speed motion-picture films of saltating flows revealed mean particle spin rates of approximately 350–400 rev/s regardless of ambient pressure. When the spin force was taken into account in numerical solutions of individual particle trajectories, using measured particle position and velocity as initial conditions in the solution, remarkable agreement between filmed and calculated trajectories was found at atmospheric pressure. However, at low pressure (0.68% of an atmosphere) the spin force was shown to have little influence on the particles' trajectories. A large percentage (20%) of particles were found to have planes of rotation differing from the vertical longitudinal one.

*Acknowledgements*—This research was supported by the NASA Ames Research Center Aeolian Consortium Group and NASA Headquarters, Office of Planetary Geology through an interchange with the University of California at Davis.

## REFERENCES

ABBOTT, J. E. & FRANCIS, J. R. D. 1977 Saltation and suspension trajectories of solid grains in a water stream. *Phil. Trans. Roy. Soc. London* **284**, 225–254.

ANDRES, R. M. 1970 The mechanics of dust lifting with particular emphasis on the planet Mars, Ph.D. dissertation, Library, St. Louis University, St. Louis, Missouri.

BAGNOLD, R. A. 1941 *The Physics of Blown Sand and Desert Dunes.* Methuen, London.

BAGNOLD, R. A. 1956 The flow of cohesionless grains in fluids. *Phil. Trans. Roy Soc. Lond.* **A249**, 235–297.

BAGNOLD, R. A. 1973 The nature of saltation and of "bedload" transport in water. *Proc. Roy. Soc. Lond.* **A332**, 473–504.

BAGNOLD, R. A. 1974 Fluid forces on a body in shear-flow; experimental use of "stationary flow". *Proc. Roy. Soc. Lond.* **A340**, 147–171.

CHEPIL, W. S. 1945 Dynamics of wind erosion. I. Nature of movement of soil by wind. *Soil Sci.* **60**, 305–320.

CHEPIL, W. S. 1958 The use of evenly spaced hemispheres to evaluate aerodynamic forces on a soil surface. *Trans. Am. Geophys. Un.* **39**, 397–403.

FRANCIS, J. R. D. 1973 Experiments on the motion of solitary grains along the bed of a waterstream. *Proc. Roy. Soc. Lond.* **A332**, 443–471.

FREE, E. E. 1911 The movement of soil material by the wind. *USDA Bur. Soils Bull.* No. 68.

GILBERT, G. K. 1914 *Transportation of debris by running water.* Department of the Interior, United States Geological Survey, Professional Paper No. 86, Washington, D. C., Government Printing Office.

GREELEY, R., WHITE, B. R., POLLACK, J. B., IVERSEN, J. D. & LEACH, R. N. 1977 *Dust storms on Mars: Considerations and simulations.* NASA TM 78423.

IVERSEN, J. D., GREELEY, R., POLLACK, J. B. & WHITE, B. R. 1973 Simulation of Marian eolian phenomena in the atmospheric wind tunnel. *Proc. AIAA/ASIM/IES/NASA, NASA Space Simulation Conference*, NASA SP-336, 191–213.

IVERSEN, J. D., GREELEY, R., WHITE, B. R. & POLLACK, J. B. 1975 Eolian erosion of the Martian surface, Part 1: Erosion rate similitude. *Icarus* **26**, 321–331.

IVERSEN, J. D., GREELEY, R., WHITE, B. R. & POLLACK, J. B. 1976 The effect of vertical distortion in the modeling of sedimentation phenomena: Martian crater wake streaks. *J. Geophys. Res.* **81**, 4846–4856.

KAWAMURA, R. 1951 *Study of sand movement by wind* (in Japanese) Tech. Res. Inst., Tokyo Univ., Tokyo, Japan, report, Vol. 5, 95–112.

MACMILLAN, F. A. 1954 Viscous effects on Pitot tubes at low speeds, *J. Aero. Soc.* **58**, 837–839.

MACMILLAN, F. A. 1956 *Experiments on Pitot tubes in shear flow.* Rep. Menor. Aero. Res. Coun. Lond. No. 3028.

MAEGLEY, W. J. 1976 Saltation and Martian sandstorms. *Rev. Geophys. & Space Sci.* **14**, 135–142.

MORSI, S. A. & ALEXANDER, A. J. 1972 An investigation of particle trajectories in two-phase flow systems. *J. Fluid Mech.* **55**, 193–208.

OWEN, P. R. 1964 Saltation of uniform grains in air. *J. Fluid Mech.* **20**, 225–242.

RADOK, U. 1968 Deposition and erosion of snow by the wind, *Res. Rep.* **230**, Cold Reg. Res. and Eng. Lab., Hanover, New Hampshire.

RUBINOW, S. & KELLER, J. 1961 The transverse force on a spinning sphere moving in a viscous fluid. *J. Fluid Mech.* **11**, 447–459.

SAGEN, C. & BAGNOLD, R. A. 1975 Fluid transport on earth and aeolian transport on Mars. *Icarus* **26**, 209–218.

SCHMIDT, R. A. 1977 *A system that measures blowing snow.* USDA Forest Service Research Paper RM-194.

TSUCHIYA, Y. 1969 Mechanics of the successive saltation of a sand particle on a granular bed in a turbulent stream, *Disa. Prev. Res. Inst. Kyoto Univ. Bull.* **19**, Part 1(152), 31–44.

WHITE, B. R. 1979a Soil transport by winds on Mars. *J. Geophys. Res.* **84**, 4643–4651.

WHITE, B. R. 1979b Low-Reynolds-number turbulent boundary layers, *Turbulent Boundary Layers: Forced, Incompressible, Non-Reacting.* (Edited by H. E. Weber), pp. 209–220. ASME, New York; also 1981 *J. Fluid Engng* **103**, 624–630.

WHITE, B. R. 1981 Venusian saltation. *Icarus* **46**, 226–232.

WHITE, B. R., GREELEY, R., IVERSEN, J. D. & Pollack, J. B. 1976 Estimated grain saltation in a Martian atmosphere. *J. Geophys. Res.* **81**, 5643–5650.

WHITE, B. R. & SCHULZ, J. C. 1977 Magnus effect in saltation. *J. Fluid Mech.* **81**, 497–512.

WILLIAMS, G. 1964 Some aspects of the eolian saltation load. *Sedimentology* **3**, 257–287.

ZINGG, A. W. 1953 Wind tunnel studies of the movement of sedimentary material. *Proc. 5th Hydraul. Conf., Bull.* 24, *Univ. Iowa Studies Engng*, pp. 111–135.